





RESEARCH ARTICLE | JUNE 22 2023

Cellularity and self-similarity of hydrogen expanding spherical flames at high pressures

Special Collection: [Hydrogen Flame and Detonation Physics](#)

Cai Xiao (蔡晓) ; Su Limin (苏利民); Wang Jinhua (王金华)  ; Hu Erjiang (胡二江); Huang Zuohua (黄佐华) 



Physics of Fluids 35, 064119 (2023)

<https://doi.org/10.1063/5.0151566>



View
Online



Export
Citation

CrossMark

Cellularity and self-similarity of hydrogen expanding spherical flames at high pressures

Cite as: Phys. Fluids **35**, 064119 (2023); doi: [10.1063/5.0151566](https://doi.org/10.1063/5.0151566)

Submitted: 23 March 2023 · Accepted: 26 May 2023 ·

Published Online: 22 June 2023



View Online



Export Citation



CrossMark

Xiao Cai (蔡晓), Limin Su (苏利民), Jinhua Wang (王金华), ^{a)} Erjiang Hu (胡二江), and Zuohua Huang (黄佐华)

AFFILIATIONS

State Key Laboratory of Multiphase Flow in Power Engineering, Xi'an Jiaotong University, Xi'an 710049, China

Note: This paper is part of the special topic, Hydrogen Flame and Detonation Physics.

^{a)} Author to whom correspondence should be addressed: jinhuaawang@mail.xjtu.edu.cn

ABSTRACT

The onset of transition to cellularity and self-similar propagation of centrally ignited, expanding spherical flames in a reactive environment of $\text{H}_2/\text{O}_2/\text{N}_2$ and $\text{H}_2/\text{O}_2/\text{He}$ mixtures at initial pressures up to 15 bar were experimentally investigated using a newly developed, constant-pressure, dual-chamber vessel and were theoretically interpreted based on linear stability theory. The experiments were well-controlled to identify the separate and coupled effects of Darrieus–Landau instability and diffusional–thermal instability. Results show that the critical radius, r_{cr} , for the onset of cellular instability varies non-monotonously with initial pressure for fuel-lean and stoichiometric $\text{H}_2/\text{O}_2/\text{N}_2$ flames. This non-monotonous pressure dependence of r_{cr} is well captured by linear stability theory for stoichiometric flames. The experimental critical Peclet number, $Pe_{\text{cr}} = r_{\text{cr}}/\delta_{\text{f}}$, increases non-linearly with the Markstein number, Ma , which measures the intensity of diffusional–thermal instability. However, a linear dependence of Pe_{cr} on Ma is predicted by linear stability theory. Specifically, the theory shows well quantitative agreement with the experimental results for mixtures with near-unity Le_{eff} ; however, it under-predicts the Pe_{cr} for mixtures with off-unity Le_{eff} . In addition, there exists three distinct propagation stages for flames subjected to cellular instability, namely, smooth expansion, transition propagation, and self-similar propagation. The acceleration exponent, α , in the self-similar propagation stage was extracted based on the power-law of $dr_{\text{f}}/dt = \alpha A^{1/\alpha} r_{\text{f}}^{(1-1/\alpha)}$, where r_{f} is the instantaneous mean flame radius, and A is a constant. The values of α are located between 1.22 and 1.40, which are smaller than the suggested value (1.5) for self-turbulization.

Published under an exclusive license by AIP Publishing. <https://doi.org/10.1063/5.0151566>

I. INTRODUCTION

Propagation of smooth laminar premixed flames are often subjected to Darrieus–Landau, hydrodynamic instability and diffusional–thermal instability, which induce cellular structures on the flame-front, in the absent of body forces. The formation of cells on the flame-front increases the total flame surface area and thus promotes the global flame propagation speed. With the enlarging and splitting of cells over the expanding flame, the flame surface area increases continuously, leading to the flame self-acceleration. It has been suggested that the flame accelerates indefinitely and could even lead to the self-turbulization of a laminar flame,^{1–3} which will play a significant role in the deflagration-to-detonation transition (DDT).^{4–8} Mechanistically, Darrieus–Landau (DL) instability wrinkles a flame through the sharp density jump across the flame-front and always occurs for very large flame or very thin flame, when the flame thickness is much thinner than the flow hydrodynamic length scale, i.e., flame radius. However, diffusional–thermal (DT) instability is controlled by the non-equidiffusive feature of heat and controlling species for a reactive

mixture. The non-equidiffusion is usually characterized by the Lewis number, Le , which is defined as the ratio of the thermal diffusivity to the mass diffusivity of the deficient reactant relative to the inert, such that the reactive mixture with $Le < 1$ de-stabilizes the flame-front, while $Le > 1$ mixture delays the cellular structure.

Due to the fundamental importance as well as practical significance, especially for high-pressure aero-engines and internal combustion engines as well as large-scale accidental gas explosions for which the Darrieus–Landau instability would be significantly enhanced, there have been substantial theoretical, numerical, and experimental studies on the cellular instabilities.^{9,10} Matalon and co-workers^{11–13} and Sivashinsky^{14,15} gradually developed the linear and nonlinear stability theories and studied the onset, growth rate, and cell size of the cellular instability. Among the numerical studies, the flame-front evolution and acceleration of 2D cylindrical and channel flames were analyzed using the Sivashinsky equation^{16–20} and the Navier–Stokes (N–S) equation.^{21–25} In addition, Bradley and co-workers,^{26–30} Law and co-workers^{31–38} as well as Huang and co-workers^{39–43} experimentally

investigated the transition from smooth to cellular flames and self-acceleration of cellular flames using large-scale open flames and high-pressure confined flames. As the onset of flame cellular instability can be determined using experimental approach and linear stability theory, it is of great interest to know whether the theory could quantitatively predict the experiment results. The previous results of Bradley *et al.*^{26,27} show that the theory underestimates the critical Peclet number for the onset of cellular instability. It was suggested that the initial growth of perturbation does not necessarily coincide with the instant that the instability is observed in the experiment due to the unsteady nature of the problem.¹³ Subsequently, Jomaas *et al.*³³ found the quantitative agreement between the experiment and the theory when the flame parameters were chosen sensibly. Specifically, the flame thickness defined based on temperature gradient and Lewis number extracted from experimental Markstein length were used in their calculations, but those are different from the original definitions used in the derivation of the theory. Beeckmann *et al.*,⁴⁴ however, stated that the theoretical findings are 4–5 times smaller than the measured critical radii for flame cellularity when the fundamental parameters follow the same definitions in the theory. Recently, Zhao *et al.*⁴² compared the experimental critical radii based on three different definitions with the theoretical results and suggested that the definition in critical radius measurements is important to reach a close agreement between the experiment and the theory.

The self-acceleration of expanding spherical flame can be quantified by the acceleration exponent, α , which would be determined by the history of flame radius, $r_f(t)$, through a power-law expression, $r_f \sim t^\alpha$. The flame radius history can be obtained using both experimental and numerical approaches. Indeed, the flame is self-acceleration if $\alpha > 1$, it is self-similar if α is a constant and holds a period of time, and it is self-turbulization if $\alpha = 1.5$.³⁴ Gostintsev *et al.*⁴⁵ analyzed the large-scale open flame experiments and found the self-similarity of the propagation flames. They concluded that the α is equal to 1.5. Nevertheless, scattered values of α were obtained in the subsequent studies,^{34,40,41,46–48} and majority of them are less than 1.5. Recently, Yang *et al.*³⁵ and Huo *et al.*³⁶ reported the transition and saturated stages. The α was measured to be larger than 1.5 in the transition stage but smaller than 1.5 in the saturated stage for all flames. Very recently, Cai *et al.*⁴³ and Kim *et al.*,⁴⁹ however, found that the α increases from the transition propagation stage to the self-similar propagation stage using high-pressure confined flames and large-scale open flames, respectively. The values of α are less than 1.5 in these two stages. Furthermore, most of the investigated flames are subjected to two modes of cellular instability, and it is still a challenge to identify the separate and coupled effects of Darrieus–Landau instability and diffusional–thermal instability on the onset of flame cellularity and self-similar propagation.

With above considerations, we are motivated to conduct well-controlled experiments to evaluate the performance of linear stability theory on the prediction of the onset of flame cellular instability and to assess the possible attainment of self-turbulization for fully developed cellular expanding spherical flames at high pressures. Systematic experiments were conducted on a newly developed, constant-pressure, dual-chamber vessel with $\text{H}_2/\text{O}_2/\text{N}_2$ and $\text{H}_2/\text{O}_2/\text{He}$ mixtures under initial pressures up to 15 bar to facilitate the Darrieus–Landau instability. In particular, the stoichiometric $\text{H}_2/\text{O}_2/\text{N}_2$ flames with $Le = 1$ were examined to study the evolution and accelerative dynamics of

Darrieus–Landau instability by suppressing the diffusional–thermal effects. Then the de-stabilizing and stabilizing effects of diffusional–thermal instability on the evolution of cellular instability were identified by investigating the fuel-lean $\text{H}_2/\text{O}_2/\text{N}_2$, fuel-rich $\text{H}_2/\text{O}_2/\text{N}_2$ as well as fuel-lean $\text{H}_2/\text{O}_2/\text{He}$ mixtures at identical flame temperature and initial pressures, but characterized by $Le < 1$ and $Le > 1$, respectively. This paper is focused on the separate and coupled effects of Darrieus–Landau instability and diffusional–thermal instability on the onset of cellular instability and the nature of flame self-acceleration at high pressures.

II. EXPERIMENTAL AND THEORETICAL METHODS

A. Experimental apparatus

All experiments were conducted in a newly developed, spark-ignition, constant-pressure, dual-chamber vessel, as shown in Fig. 1. The details of the experimental apparatus were described in Refs. 50 and 51. The vessel consists of two concentric chambers, as shown in Fig. 1(b). The inner diameters of the inner and outer chambers are 140 and 500 mm, respectively. Eight one-way valves are mounted on the inner chamber to allow gas enter the outer chamber when the inner

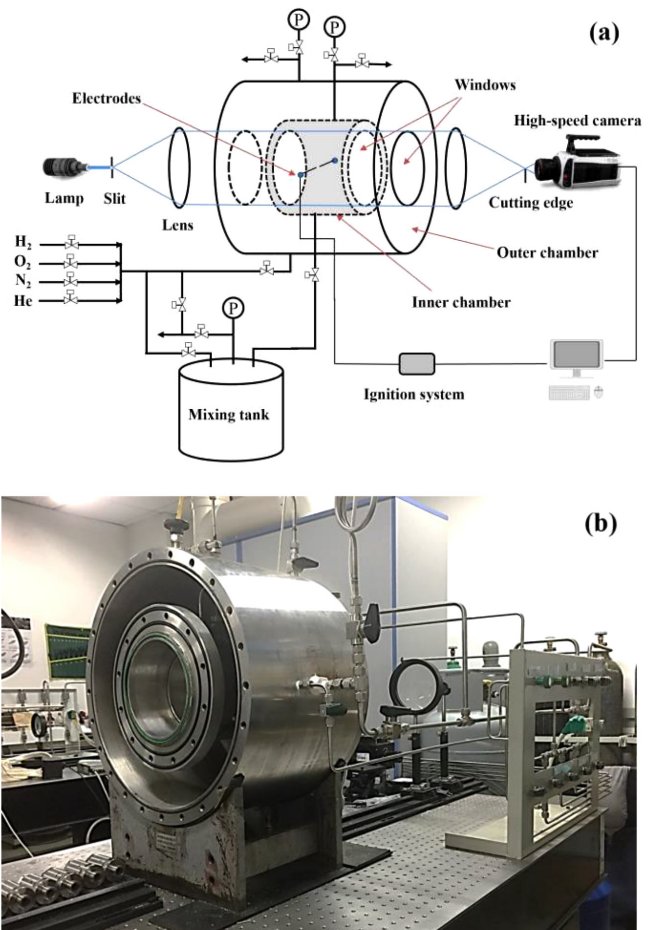


FIG. 1. Experimental setup: (a) schematic configuration of the system and (b) experimental apparatus.

pressure is slightly higher than the outer pressure. In experiments, the inner chamber is filled with combustible mixture, while the outer chamber is filled with inert gas, such as nitrogen. The combustible mixture is prepared in a 71.1 l mixing tank based on partial pressures. Then, the pure nitrogen and premixed combustible mixture are filled in the outer and inner chamber, respectively, and the pressure difference keeps small during the filling process. The combustible mixture is ignited after waiting several minutes to ensure a quiescence environment in the inner chamber. The 8 one-way valves are opened, and the inner and outer chambers are connected during the flame propagation event. Two quartz windows with optical diameter of 120 mm are located at two ends of the vessel. The expanding spherical flame is imaged using Schlieren photography with a high-speed camera (Phantom v611) at 10 kHz and resolution of 752×752 pixels. The instantaneous mean flame radius, $r_f = (A_f/\pi)^{0.5}$, was determined based on the enclosed area of the flame (A_f), which was widely used in cellular flames.^{36,43} The instantaneous flame propagation speed based on the burned mixture was calculated by $S_b = dr_f/dt$. It is noted that only data within 5 to 25 mm were processed to eliminate the effects of ignition and chamber confinement.^{52–54}

B. Experimental conditions and computational methods

Since we are interested in the pure Darrieus–Landau (DL) instability as well as diffusional–thermal (DT) de-stabilizing and stabilizing effects on the Darrieus–Landau instability, the experimental conditions were chosen such that the adiabatic flame temperature (T_{ad}) remains 1600 K, and thus the density ratio (σ) is almost identical. Three typical $H_2/O_2/N_2$ mixtures with different effective Lewis numbers (Le_{eff}) defined as the ratio between the thermal diffusivity to the mass diffusivity were selected to study the pure DL instability ($\phi = 1.00$, $Le_{eff} = 1$), DT de-stabilizing effect on DL instability ($\phi = 0.60$, $Le_{eff} < 1$), and DT stabilizing effect on DL instability ($\phi = 1.50$, $Le_{eff} > 1$). Furthermore, as the inert gas would also affect the Le_{eff} of the mixture, a fuel-lean

$H_2/O_2/He$ mixture ($\phi = 0.85$) with $Le_{eff} > 1$ was also investigated. The detailed experimental conditions and fundamental parameters are listed in Table I. The initial pressures are mainly set as 5, 10, and 15 bar to promote the development of hydrodynamic cells.

The fundamental parameters, such as the laminar burning velocity (S_L), laminar flame thickness (δ_f), adiabatic flame temperature (T_{ad}), and density ratio (σ), for investigated flames were calculated using the 1D freely propagation flame and equilibrium code in the Chemkin-Pro software, with the chemical kinetic mechanism of Burke *et al.*⁵⁵ The laminar flame thickness is determined based on thermal diffusion, $\delta_f = \alpha/S_L = (\lambda/\rho_u c_p)/S_L$, which was used in the derivation of linear stability theory.^{12,13} The α is the thermal diffusion; λ and c_p are the thermal conductivity and the specific heat capacity of unburnt mixture. The effective Lewis numbers (Le_{eff}) are calculated based on the expression of Matalon and co-workers^{12,56}

$$Le_{eff} = 1 + \frac{(Le_E - 1) + (Le_D - 1)\mathcal{A}}{1 + \mathcal{A}}, \tag{1}$$

where Le_E and Le_D are the Lewis numbers of excess and deficient reactants, respectively. $\mathcal{A} = 1 + Ze(\Phi - 1)$ represents the mixture’s strength. The Φ is equal to the ϕ for fuel-rich mixtures and is $1/\phi$ for fuel-lean mixtures. The Zeldovich number, $Ze = E_a(T_{ad} - T_u)/\mathcal{R}T_{ad}^2$,⁵⁷ is based on the global activation energy, $E_a = -2\mathcal{R} \left[\frac{\partial \ln(\rho_u S_L)}{\partial \ln(1/T_{ad})} \right]_{p, \phi}$, where \mathcal{R} is universal gas constant. The details of the determination of E_a were reported in previous works of Law and co-workers.^{33,57}

C. Linear stability theory

Linear stability theory develops gradually for both planar flames and expanding spherical flames. A theoretical description of the onset of cellular instability for expanding spherical flame was given by Istratov and Librovovich,⁵⁸ based on a Darrieus–Landau model with Markstein correction, and later by Bechtold and Matalon,¹¹ who incorporated hydrodynamic and diffusional–thermal effects in a more systematic way based on a hydrodynamic model. Subsequently,

TABLE I. Experimental conditions and fundamental parameters of hydrogen flames. p : initial pressure; ϕ : equivalence ratio; $X(i)$: mole fractions of species i ($i = H_2, O_2, N_2, He$); S_L : laminar burning velocity, σ : density ratio; δ_f : laminar flame thickness; Le_{eff} : effective Lewis number. Adiabatic flame temperature (T_{ad}) and initial temperature (T_u) are 1600 and 298 K, respectively.

p (bar)	ϕ	$X(H_2)$	$X(O_2)$	$X(N_2)$	$X(He)$	S_L (cm/s)	σ	δ_f (mm)	Le_{eff}
1	0.60	0.1671	0.1393	0.6936	0.0000	40.4	4.92	0.0884	0.56
2	0.60	0.1671	0.1393	0.6936	0.0000	30.6	4.92	0.0584	0.56
5	0.60	0.1671	0.1393	0.6936	0.0000	18.0	4.92	0.0396	0.56
10	0.60	0.1671	0.1393	0.6936	0.0000	9.5	4.92	0.0377	0.56
2	1.00	0.1667	0.0833	0.7500	0.0000	29.1	4.92	0.0611	1.07
5	1.00	0.1667	0.0833	0.7500	0.0000	16.4	4.92	0.0435	1.07
10	1.00	0.1667	0.0833	0.7500	0.0000	8.3	4.92	0.0428	1.07
5	1.50	0.2483	0.0828	0.6689	0.0000	63.3	4.92	0.0134	1.79
10	1.50	0.2483	0.0828	0.6689	0.0000	41.3	4.92	0.0103	1.79
15	1.50	0.2483	0.0828	0.6689	0.0000	29.0	4.92	0.0098	1.79
5	0.85	0.1197	0.0704	0.0000	0.8099	66.8	5.08	0.0439	1.18
10	0.85	0.1197	0.0704	0.0000	0.8099	47.0	5.08	0.0312	1.18
15	0.85	0.1197	0.0704	0.0000	0.8099	33.9	5.08	0.0289	1.18

20 July 2023 09:53:41

Addabbo *et al.*¹² generalized the results to allow for temperature dependence transport coefficients and a wide range of ϕ . The smooth spherical flame-front can be expressed as $r = r_f(t)$. The perturbed spherical flame-front can then be written as $r = r_f(t)[1 + A(t)S_n(\theta, \varphi)]$, where $A(t)$ is the amplitude of the perturbation; $S_n(\theta, \varphi)$ is the spherical surface harmonics. θ and φ are the polar and azimuth angles of a spherical coordinate. Therefore, the non-dimensional growth rate, Σ of amplitude, $A(t)$ of the perturbation of wavenumber, n can be expressed as^{12,26}

$$\Sigma = \frac{2\pi\sigma}{n} \left(1 - \frac{2Ma}{Pe}\right) \left(\omega_{DL} - \frac{\Omega}{Pe}\right), \quad (2)$$

$$\Omega = \Omega_1 + \frac{Ze(Le_{eff} - 1)}{\sigma - 1} \Omega_2 + Pr\Omega_3, \quad (3)$$

where $Pe = r_f/\delta_f$ is the Peclet number, and $Ma = L/\delta_f$ is the Markstein number. The theoretical Markstein length, L , is based on the realistic choice of the temperature dependence thermal conductivity of the mixture, and $\lambda = T^{0.5}$ is given by the following expression:¹²

$$L = \delta_f \left\{ \frac{2}{\sqrt{\sigma} + 1} + \frac{2Ze(Le_{eff} - 1)}{\sigma - 1} \left[\sqrt{\sigma} - 1 - \ln \frac{\sqrt{\sigma} + 1}{2} \right] \right\}. \quad (4)$$

It should be noted that the finite front-thickness effects are parameterized by different Markstein lengths relative to the flame stretch, strain, curvature, and compression.⁵⁹ For the expanding spherical flames, flame curvature and total stretch rate are proportional to each other, a single Markstein length merges.^{56,60}

The ω_{DL} in Eq. (2) represents the de-stabilizing effect of Darrieus–Landau instability, whereas the Ω/Pe represents the influences of transport, i.e., thermal conduction, molecular diffusion, and viscous diffusion as expressed in Eq. (3). The ω_{DL} , Ω_1 , Ω_2 , and Ω_3 depend only on σ and n and are given in the previous work.¹² The Prandtl number is set as $Pr = 0.75$ in the calculations.

A flame can become unstable if the growth rate of at least one wavenumber is positive. The theoretical critical Peclet number, Pe_{cr} , for the onset of flame cellular instability would be derived by setting the right-hand-side of Eq. (2) to zero

$$Pe_{cr} = \frac{\Omega}{\omega_{DL}} = \omega_{DL}^{-1} \left[\Omega_1 + \frac{Ze(Le_{eff} - 1)}{\sigma - 1} \Omega_2 + Pr\Omega_3 \right]. \quad (5)$$

The first term in the right-hand-side of Eq. (5), Ω_1/ω_{DL} , represents the “base” hydrodynamic boundary between the stretch-affected stable and unstable regimes,³³ while the second term describes the diffusional–thermal effects, and the third term characterizes the viscous diffusion effects. The detailed flame parameters to determine the theoretical critical Peclet number for the hydrogen flames under different conditions are listed in Table II.

III. RESULTS AND DISCUSSIONS

A. Morphology and flame propagation speed

Three typical high-speed image sequences of expanding spherical $H_2/O_2/N_2$ flames at different initial pressures and equivalence ratios are shown in Fig. 2. The instantaneous mean flame radii of the images are from 10 to 40 mm with an interval of 10 mm in different rows. It is seen that the stoichiometric hydrogen flame is stable at 2 bar in the initial stage of propagation, large cracks form on the smooth flame-front,

TABLE II. The detailed flame parameters to determine the critical Peclet number from linear stability theory for the hydrogen flames under different conditions. Pe_1 , Pe_2 , and Pe_3 : hydrodynamic, diffusional–thermal, and viscous diffusion terms in Eq. (5); Pe_{cr} : critical Peclet number for the onset of cellular instability.

p (bar)	ϕ	diluent	Ω_1	Ω_2	$Ze(Le_{eff} - 1)$	Pe_1	Pe_2	Pe_3	Pe_{cr}
1	0.60	N_2			−3.6				/
2	0.60	N_2			−4.3				/
5	0.60	N_2			−5.4				/
10	0.60	N_2			−8.8				/
2	1.00	N_2	238	339	0.6	159	36	11	207
5	1.00	N_2	241	343	0.8	159	45	11	216
10	1.00	N_2	241	344	1.1	159	61	11	232
5	1.50	N_2	260	368	7.0	159	405	12	576
10	1.50	N_2	264	373	9.5	160	546	12	717
15	1.50	N_2	268	379	11.4	160	658	12	829
5	0.85	He	249	366	1.7	161	97	11	269
10	0.85	He	249	366	1.8	161	106	11	278
15	0.85	He	249	366	1.9	160	109	11	280

and cells evoke spontaneously and appear uniformly over the entire flame surface as the flame propagates outwardly. The cellular structure appears earlier at higher pressure (5 bar) due to the development of Darrieus–Landau instability for thinner flame. For fuel-lean ($\phi = 0.60$) hydrogen flame at 5 bar, the flame-front is highly wrinkled, and additional small-scale diffusional–thermal cells develop on the larger hydrodynamic cells, see the zoom-in image in the last row. This reveals the de-stabilizing effect of the diffusional–thermal instability on fuel-lean hydrogen flame with $Le_{eff} < 1$. Figure 3 presents a set of image sequences of $H_2/O_2/N_2$ and $H_2/O_2/He$ flames at 10 bar to illustrate the stabilizing effect of diffusional–thermal instability. It is observed that stoichiometric hydrogen flame at 10 bar is highly unstable with small Darrieus–Landau cells on the flame-front. While the fuel-rich ($\phi = 1.50$) hydrogen flame is stable at small flame radius, it becomes unstable at large flame radius with relative larger Darrieus–Landau cells covering the entire flame surface. As the fuel-rich hydrogen flame has the same density ratio and smaller flame thickness ($\sigma = 4.92$, $\delta_f = 0.0103$ mm) compared with the stoichiometric hydrogen flame ($\sigma = 4.92$, $\delta_f = 0.0428$ mm), it should be more susceptible to hydrodynamic instability. Thus, the delay of the formation of cellular structure should be attributed to the stabilizing effect of diffusional–thermal instability ($Le_{eff} > 1$) on the development of Darrieus–Landau cells. This stabilizing effect is further demonstrated by the fuel-lean $H_2/O_2/He$ flame ($Le_{eff} > 1$) with similar hydrodynamic instability (with similar σ and δ_f) to the stoichiometric $H_2/O_2/N_2$ flame. The hydrogen flame in helium is more stable than fuel-rich hydrogen flame as only large cracks develop on the flame-front within the present observation range.

The formation of cellular structures on the flame-front can increase the total flame surface area and thus increases the flame propagation speed. The cascade development of cells continuously promotes the flame propagation speed and would lead to the self-similar propagation. Figure 4 plots the normalized flame propagation speed, $\bar{S}_b = S_b/(\sigma S_L)$ vs the Peclet number, $Pe = r_f/\delta_f$ for $H_2/O_2/N_2$ and $H_2/O_2/He$ flames at different initial pressures and equivalence ratios. For stoichiometric $H_2/O_2/N_2$ mixture with unity Le_{eff} , the

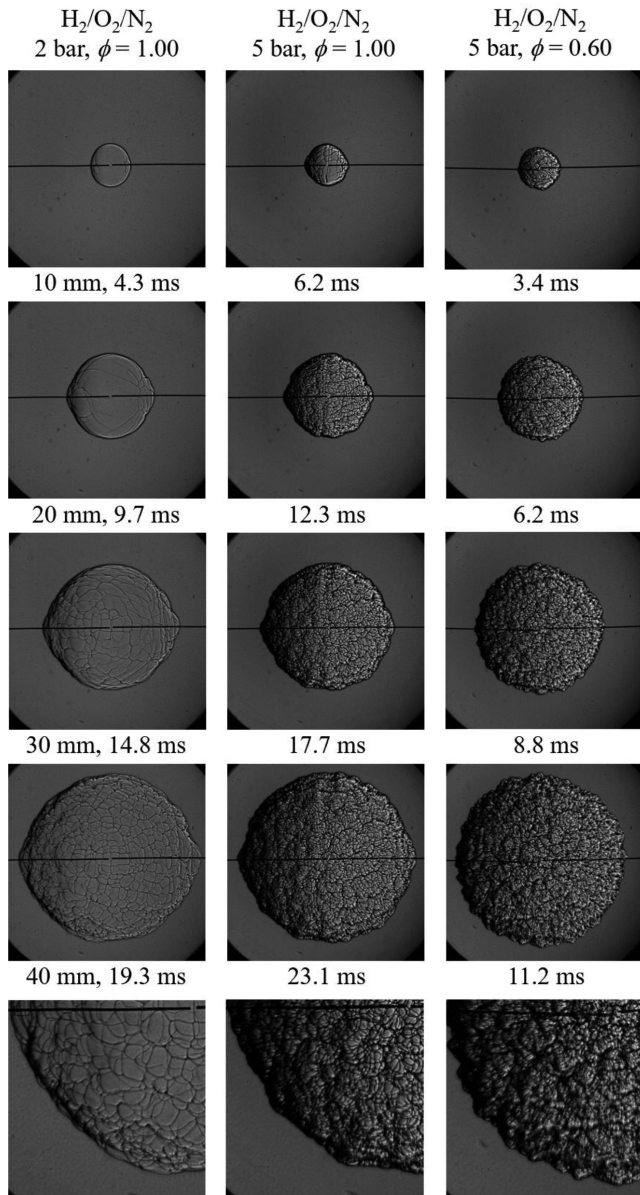


FIG. 2. Flame-front images for expanding spherical $H_2/O_2/N_2$ flames at different initial pressures and equivalence ratios. Zoom-in images in the last row.

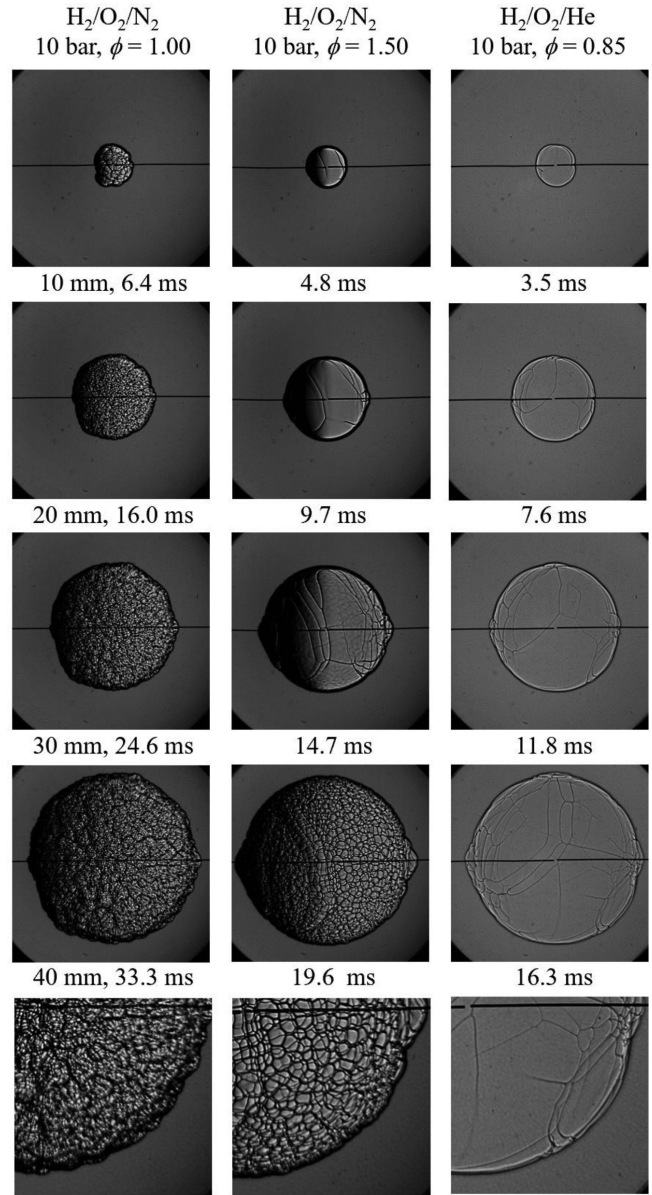


FIG. 3. Flame-front images for expanding spherical $H_2/O_2/N_2$ and $H_2/O_2/He$ flames at 10 bar and different equivalence ratios. Zoom-in images in the last row.

flames are smooth without any cellular structure for $Pe < 200$, and the $\overline{S_b}$ almost keeps constant. This stage is suggested as the smooth expansion stage. As flame expands, the large cracks develop and cellular instability evokes on the flame-front when the Pe exceeds a critical value, i.e., $Pe_{cr} \approx 200$, and the flame accelerates rapidly due to the increasing and splitting of hydrodynamic cells, hereafter termed as the transition propagation stage. When the smallest hydrodynamic cell reaches an inner cutoff limit, a moderate flame acceleration is observed. The slope in the log-plot of $\overline{S_b} - Pe$ is almost constant in this

period, thus referred to as the self-similar propagation stage. The three distinct propagation stages were also reported in previous works.^{35,36,43} For fuel-lean $H_2/O_2/N_2$ flames with sub-unity Le_{eff} , three propagation stages are also observed, and the $\overline{S_b}$ increases for mixture with $Le_{eff} < 1$, which is the consequence of the development of small diffusional-thermal cells on the hydrodynamic cells. While the $\overline{S_b}$ almost keeps constant in the radii range between 5 and 25 mm for fuel-rich $H_2/O_2/N_2$ fuel-lean $H_2/O_2/He$ flames with $Le_{eff} > 1$, implying that the diffusional-thermal effects damp the development of the hydrodynamic cells.

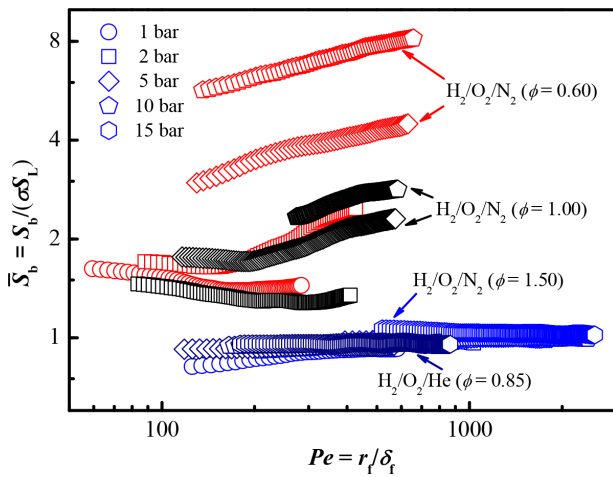


FIG. 4. Propagation of $\text{H}_2/\text{O}_2/\text{N}_2$ and $\text{H}_2/\text{O}_2/\text{He}$ expanding spherical flames at different initial pressures and equivalence ratios. $S_b = S_b/(\sigma S_L)$ is the normalized flame propagation speed. $Pe = r_f/\delta_f$ is the flame Peclet number.

B. Theoretical growth rate and neutral stability curve

Figure 5(a) shows the non-dimensional growth rate, Σ at the critical wavenumber, $n_{cr} = 13$, and flame radius of 10 mm for hydrogen flame at different initial pressures, equivalence ratios, and diluents. The growth rate of stoichiometric ($\phi = 1.00$) $\text{H}_2/\text{O}_2/\text{N}_2$ flames (black curve) is negative at ambient pressure, indicating that the flame is hydrodynamically stable with thick flame thickness. It gradually increases with the initial pressure and becomes positive at higher pressures. The Darrieus–Landau instability is expected to be significant with decreasing flame thickness, and flame becomes unstable at higher pressure, see image I. However, the growth rate decreases with the initial pressure when it exceeds a critical value, which is attributed to the thicker flame thickness caused by three-body reaction at very high pressure. For fuel-lean ($\phi = 0.60$) $\text{H}_2/\text{O}_2/\text{N}_2$ flames (red curve), the growth rate is always positive due to the de-stabilizing effect of diffusional–thermal instability. Specifically, the flame-front is covered by irregularity cells with different sizes at ambient pressure (see image II), and it becomes diffusional–thermal unstable. However, the flame-front is highly wrinkled with the development of both diffusional–thermal and hydrodynamic cells at higher pressure (see image III). For fuel-rich ($\phi = 1.50$) $\text{H}_2/\text{O}_2/\text{N}_2$ and fuel-lean ($\phi = 0.85$) $\text{H}_2/\text{O}_2/\text{He}$ mixtures with $Le_{eff} > 1$, the flames are expected to be more stable as the development of hydrodynamic cells is damped by diffusional–thermal effects, see images IV and V. It is observed that the fuel-rich $\text{H}_2/\text{O}_2/\text{N}_2$ flame ($Le_{eff} = 1.8$) at 5 bar is covered with uniform hydrodynamic cells, while the fuel-lean $\text{H}_2/\text{O}_2/\text{He}$ flame ($Le_{eff} = 1.2$) remains smooth without any cellular structure. It would be attributed to the thicker flame thickness for $\text{H}_2/\text{O}_2/\text{He}$ flame and smaller Pe , and thus, the ω_{DL} term decreases and the Ω/Pe term increases in Eq. (2). Therefore, the $\text{H}_2/\text{O}_2/\text{He}$ flame is more cellular stable.

The onset of flame cellular instability and the range of cell size developed on the flame-front can be theoretical deduced from Eq. (2) in the form of a neutral stability curve, as shown in Fig. 6. The neutral stability curve is obtained by setting the right-hand-side of Eq. (2) to zero. The map shows the range of unstable wavenumber, n , as a

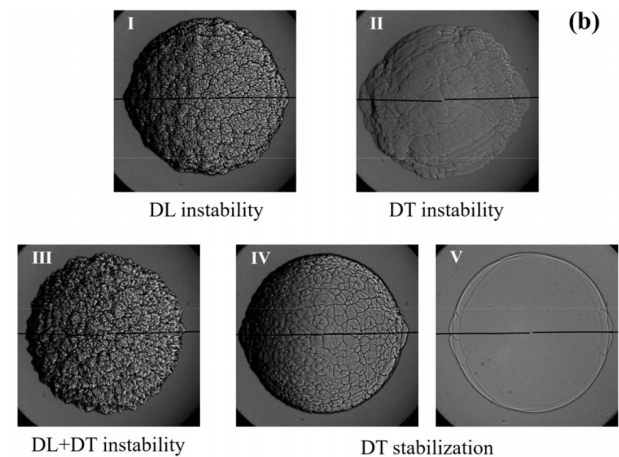
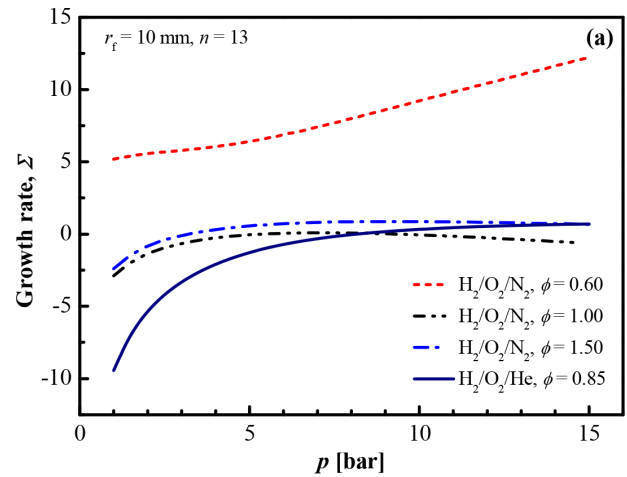


FIG. 5. (a) Theoretical growth rate with initial pressure for hydrogen flames and (b) typical flame images. The flame radius of the images is about 40 mm. I: $\text{H}_2/\text{O}_2/\text{N}_2$ mixture at $\phi = 1.00$ and $p = 5$ bar; II: $\text{H}_2/\text{O}_2/\text{N}_2$ mixture at $\phi = 0.60$ and $p = 1$ bar; III: $\text{H}_2/\text{O}_2/\text{N}_2$ mixture at $\phi = 0.60$ and $p = 5$ bar; IV: $\text{H}_2/\text{O}_2/\text{N}_2$ mixture at $\phi = 1.50$ and $p = 5$ bar; and V: $\text{H}_2/\text{O}_2/\text{He}$ mixture at $\phi = 0.85$ and $p = 5$ bar.

function of the Peclet number. The nose of the peninsula determines the critical Peclet number, Pe_{cr} , for the onset of flame cellular instability.¹² The regime within the peninsula predicts that the cell size falls in the range of unstable wavelength, $\lambda_{min} < \lambda < \lambda_{max}$ at a given Peclet number (or flame radius), with the larger corrugations ($\lambda > \lambda_{max}$) stabilized by flame stretch and smaller disturbances ($\lambda < \lambda_{min}$) stabilized by diffusion.¹³ The lower branch of the peninsula decreases and asymptotes to $n^* = 6.2$, which is characterized by purely hydrodynamic effect. Thus, the largest cell size, $\lambda_{max} = 2\pi r_f/n^*$, increases linearly with the flame radius. The upper branch of the peninsula asymptotes to a line, $Pe/n = \Gamma$, which depends on the Le_{eff} and σ . Hence, the smallest cell size, $\lambda_{min} = 2\pi r_f/n = 2\pi\Gamma\delta_f$ depends of the flame thickness and mixture composition. It was suggested that λ_{min} represents the averaged cell size of the flame with fully developed cellular structures.¹³ From Fig. 6(a), the neutral stability curve moves slightly when the initial pressure increases from 2 to 10 bar for

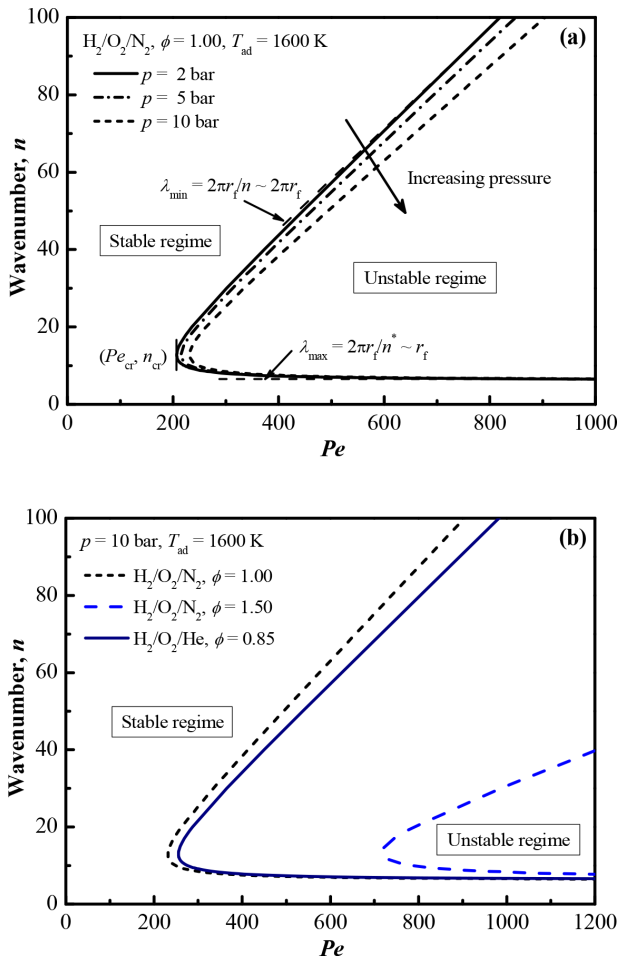


FIG. 6. Peninsula of unstable modes as a function of Peclet number of hydrogen flames: (a) stoichiometric $H_2/O_2/N_2$ mixture at 2, 5, and 10 bar and (b) stoichiometric and fuel-rich $H_2/O_2/N_2$ mixtures and fuel-lean $H_2/O_2/He$ mixture at 10 bar.

stoichiometric $H_2/O_2/N_2$ mixture. It suggests that the Pe_{cr} is insensitive to initial pressure for stoichiometric mixture. However, the nose of the peninsula is significantly delayed for fuel-rich $H_2/O_2/N_2$ mixture, as shown in Fig. 6(b). This is because the diffusional–thermal term, $\frac{Ze(L_{eff}-1)}{\sigma-1}\Omega_2$ in Eq. (5), increases notably as the $Le_{eff} = 1.8$ for fuel-rich mixture. In addition, the slope of the upper of the peninsula decreases, indicating that the normalized smallest cell size, $\lambda_{min}/\delta_f = 2\pi\Gamma$ increases. Therefore, the averaged cell size would be possibly measured for flame with large Le_{eff} at high pressure.

C. Onset of flame cellular instability

Figure 7(a) shows the critical Peclet number, Pe_{cr} , for the onset of cellular instability as a function of initial pressure for hydrogen flames. The Pe_{cr} is extracted from the neutral stability curve or the Eq. (5). Since the Le_{eff} and $Ze(L_{eff}-1)$ of fuel-rich ($\phi = 1.50$) $H_2/O_2/N_2$ flame is larger than that of stoichiometric ($\phi = 1.00$) $H_2/O_2/N_2$ and fuel-lean ($\phi = 0.85$) $H_2/O_2/He$ flames, the Pe_{cr} is notably larger for fuel-rich $H_2/O_2/N_2$ flames at different initial pressures. It is seen that the Pe_{cr} is

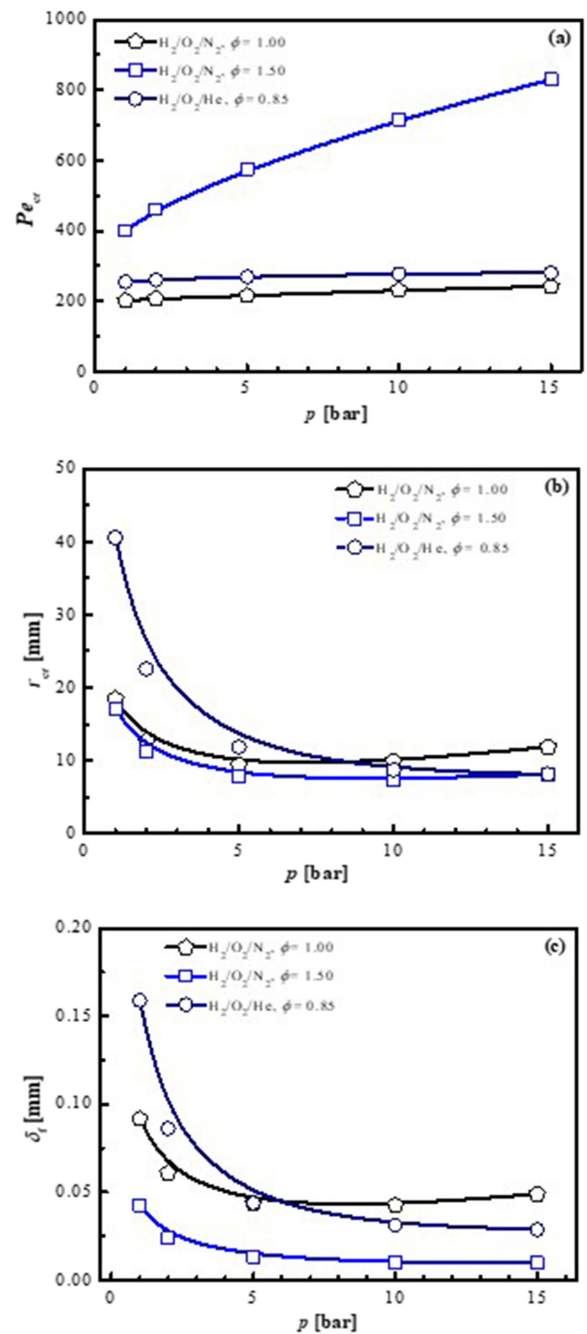


FIG. 7. Theoretical critical Peclet number (a) and flame radius (b) for the onset of cellular instability and flame thickness (c) for stoichiometric ($\phi = 1.00$) and fuel-rich ($\phi = 1.50$) $H_2/O_2/N_2$ mixture and fuel-lean ($\phi = 0.85$) $H_2/O_2/He$ mixture at different pressures.

insensitive to the initial pressure for both stoichiometric $H_2/O_2/N_2$ and fuel-lean $H_2/O_2/He$ mixtures, which is observed in the neutral stability curve in Fig. 6(a). The similar result was also reported in previous H_2 /air flames at $P = 2-5$ bar.³⁶ However, the Pe_{cr} for fuel-rich

H₂/O₂/N₂ mixture increases gradually with the initial pressure. It would be attributed to the increasing Ze and $Ze(Le_{eff}-1)$ with the initial pressure, and the stabilizing effect of diffusional–thermal instability is promoted at higher pressure for fuel-rich H₂/O₂/N₂ mixture. It should be noted that the Ze also increases with initial pressure for other two mixtures. However, the $Ze(Le_{eff}-1)$ of these flames is small, and thus, the Pe_{cr} becomes insensitive to the initial pressure.

The theoretical critical radius, r_{cr} , for the onset of flame cellular instability can be obtained by the product of Pe_{cr} and δ_f as shown in Fig. 7(b). The laminar flame thickness calculated based on the thermal diffusion,⁶¹ $\delta_f = \alpha/S_L = (\lambda/\rho_u c_p)/S_L$, is plotted in Fig. 7(c). It is observed that the r_{cr} decreases significantly with the initial pressure from 1 to 5 bar for all mixtures due to the thin flame thickness at higher pressure. However, the r_{cr} increases slightly at high pressure for stoichiometric H₂/O₂/N₂ flames. This is because the three-body reaction, $H+O_2(+M) = HO_2(+M)$, becomes important at high pressure, the δ_f increases slightly with initial pressure, and thus, the theoretical r_{cr} at 10 and 15 bar are larger than that at 5 bar.

Since we are interested in the de-stabilizing and stabilizing effects of diffusional–thermal instability on the onset of flame cellular instability, the dependence of the critical Peclet number, Pe_{cr} , on the Markstein number, Ma , is investigated. Figure 8 plots the calculated and measured Markstein number as a function of the initial pressure for H₂/O₂/N₂ and H₂/O₂/He flames at different equivalence ratios. The theoretical $Ma = L/\delta_f$ is determined based on Eq. (4). The experimental Ma relative to burned gas is measured using a non-linear stretch extraction method (LC method),⁵³ $S_b = S_b^0 - 2L_b/r_f$ from the smooth expanding flames, where S_b and S_b^0 are stretched and unstretched flame propagation speeds relative to burned gas, respectively. The experimental $Ma = L_b/\delta_f$ is obtained based on the measured Markstein length relative to burned gas, L_b . It is seen that the experimental results are larger than the theoretical predictions. A good qualitative agreement is achieved between the experiment and the theory. It should be noted that the experimental measurement of L_b is very sensitive to the definition of flame radius or iso-surface^{60,62} and the perturbation in the flame propagation. The flame radii defined

TABLE III. Measured and calculated laminar burning velocities and Marksetin numbers of hydrogen flames at different initial pressures and equivalence ratios. Experimental S_L and Ma are extracted using LC method.⁵³ Numerical S_L is obtained with Burke Mech.⁵⁵ Theoretical Ma is calculated from Eq. (4).

p (bar)	ϕ	diluent	S_L (cm/s)		Ma	
			Exp.	Numer.	Exp.	Theor.
1	1.50	N ₂	96.9	100.0	3.60	2.13
2	1.50	N ₂	87.4	88.0	3.93	2.52
5	1.50	N ₂	64.0	63.3	4.15	3.28
10	1.50	N ₂	42.0	41.3	5.04	4.21
5	0.85	He	63.5	66.8	2.20	1.25
10	0.85	He	46.1	47.0	2.26	1.30
15	0.85	He	32.9	33.9	2.13	1.32

based on the enclosed area of the flame and the circle fitting of the flame were tested, and similar results were obtained (not shown here). For consistency, the flame radius for both smooth and cellular flames is defined based on the flame area method in the present work. This is because the experimental Ma can be determined under limited conditions ($Le_{eff} > 1$ flames), and the theoretical Ma will be used in the following discussions. In addition, the measured S_L and Ma are compared with the calculated results in Table III. It is seen that the numerical S_L well predicts the experimental data under present conditions.

It is seen that the theoretical Ma decreases and increases gradually with the initial pressure for flames with $Le_{eff} < 1$ and flames with $Le_{eff} > 1$, respectively. It almost keeps constant at different initial pressures for near-unity Le_{eff} mixture. This is because the Le_{eff} and σ are insensitive to the initial pressure; the Ze , however, increases gradually with the initial pressure. The absolute value of Markstein number, $|Ma|$, increases gradually with the initial pressure for off-unity Le_{eff} flames and almost keeps constant for near-unity Le_{eff} flames based on Eq. (4). The dependence of the critical Peclet number on the Markstein number is presented in Fig. 9. It is observed that the

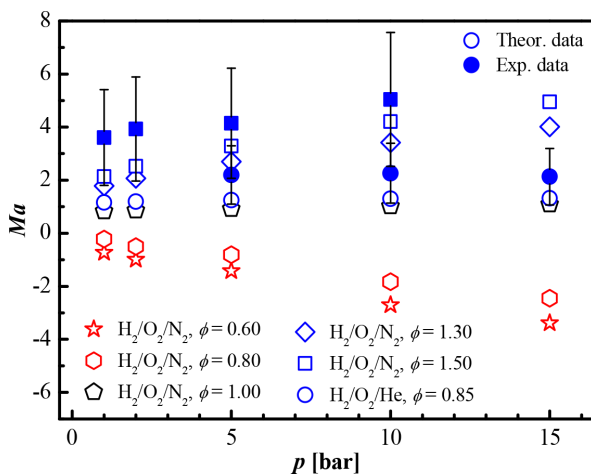


FIG. 8. Calculated and measured Markstein number as a function of initial pressure for H₂/O₂/N₂ and H₂/O₂/He mixtures with different equivalence ratios.

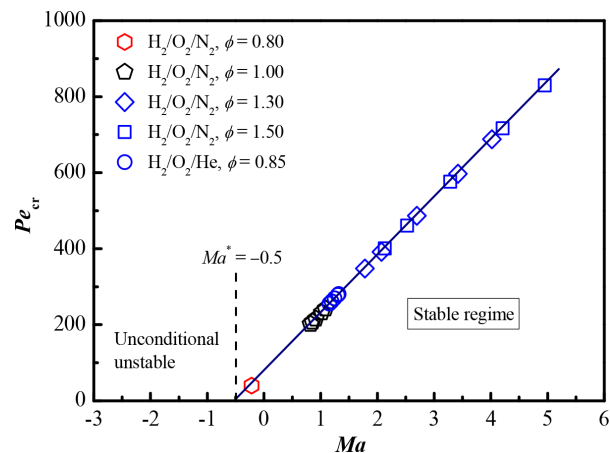


FIG. 9. Dependence of theoretical critical Peclet number on the Markstein number for hydrogen cellular expanding flames.

theoretical Pe_{cr} increases linearly with the theoretical Ma . The Ma measures the strength of diffusional–thermal effect, while the Pe_{cr} characterizes the extent of cellular instability. The results suggest that the flame cellular instability is strongly affected by the diffusional–thermal effect. The onset of cellular instability will be delayed (or enhanced) for flame with large Ma (or small Ma). The linear stability theory predicts that the flame is unconditional unstable for mixture with $Ma < Ma^* = -0.5$. In other words, the flame will become cellular unstable when it is ignited.

The experimental critical radius for the onset of cellular instability can be determined from the spherical expanding flames based on flame images or flame propagation speeds. In this study, one r_{cr} is defined based on the rapid increase in the flame propagation speed in a $S_b - (2/r_f)(dr_f/dt)$ curve, where S_b is the flame propagation speed, and $(2/r_f)(dr_f/dt)$ measures the flame stretch, K for smooth flame, as shown in Fig. 10(a). This definition was widely used in previous works,^{29,43} thus termed as critical radius for flame acceleration. The other r_{cr} is defined as the instant that cells appear spontaneously and uniformly

over the entire flame surface based on the Schlieren images, which was also widely applied in experimental measurements,^{33,63} hereafter termed as critical radius for flame cellularity. The uncertainty on the measurements of r_{cr} is mainly from the personal equation in determining the critical instant of the rapid increase in S_b or the critical radius of the uniformed global cell formation, the flame radius extraction error from the image, and the random error. The personal equation depends on the camera frame rate and S_b , which is estimated to be 0.21–0.55 mm for r_{cr} of flame acceleration and 0.32–1.23 mm for r_{cr} of flame cellularity. The flame radius extraction error is determined by the image resolution and Canny edge detection, which is estimated to be 0.28 mm. However, the random error is determined by the variation in different runs for each condition. The total uncertainty of r_{cr} is estimated to be 0.84–1.82 mm for flame acceleration, and it is estimated to be 1.27–2.71 mm for flame cellularity.

The experimentally measured r_{cr} for flame acceleration for fuel-lean and stoichiometric $H_2/O_2/N_2$ flames at different initial pressures are plotted in Fig. 10(b), which shows a slightly non-monotonous variation in r_{cr} with increasing initial pressure. The linear stability theory well captures the pressure dependence of the r_{cr} for stoichiometric flames. It is seen that the experimentally measured values largely agree with the theoretical results. The slightly non-monotonous pressure dependence of the r_{cr} could be attributed to the slightly improvement of DT stabilization effect and non-monotonous variation of DL instability. Specially, the Pe_2 increases slightly with initial pressure, while the Pe_1 keeps constant, and the δ_f varies non-monotonously with initial pressure, as shown in Table II and Fig. 7(c). In addition, the experimental r_{cr} for H_2 /air flames at different equivalence ratios and initial pressures from Huo *et al.*⁶⁴ are compared with the present results. It is found that the previous data are consistent with the current measurements, see Fig. 10(b).

Figure 11 shows the comparison of the experimental and theoretical critical radius and critical Peclet number for the onset of flame cellular instability. Both the r_{cr} for flame acceleration and r_{cr} for flame cellularity are plotted in Fig. 11(a), and the former r_{cr} is smaller than the later r_{cr} , which was also observed in the previous work.⁴² Because the r_{cr} for flame acceleration defined based on the $S_b - (2/r_f)(dr_f/dt)$ curve is suggested to largely characterize the branching of large cracks on the flame-front.⁴² It is seen that linear stability theory well predicts the r_{cr} for flame acceleration for stoichiometric $H_2/O_2/N_2$ flames with $Le_{eff} = 1$, which was discussed in the preceding paragraph. Nevertheless, the theory under-predicts the r_{cr} for flame acceleration for off-stoichiometric hydrogen flames with $Le_{eff} > 1$ or $Le_{eff} < 1$. As the values of Ma for fuel-lean $H_2/O_2/N_2$ flames are less than $Ma^* = -0.5$, these flames are predicted to be unconditional unstable; in other words, the values of the theoretical r_{cr} are zero for these flames with $Le_{eff} < 1$. Figure 11(b) compares the experimental and theoretical Pe_{cr} . In general, both experimental and theoretical Pe_{cr} increase with the theoretical Ma . However, the experimental Pe_{cr} increases non-linearly with the Ma , while the theoretical Pe_{cr} gives a linear increase trend with the Ma . The non-linear dependence of the Pe_{cr} on the Ma was also reported in recent experimental works.^{30,43} It is observed that a quantitative agreement between experimental Pe_{cr} and theoretical prediction is achieved only under limited conditions, i.e., stoichiometric $H_2/O_2/N_2$ flames with near-unity Le_{eff} . However, the theory underestimates the Pe_{cr} for off-unity Le_{eff} flames. Beekmann *et al.*⁴⁴ reported that linear stability theory under-predicts the critical radius

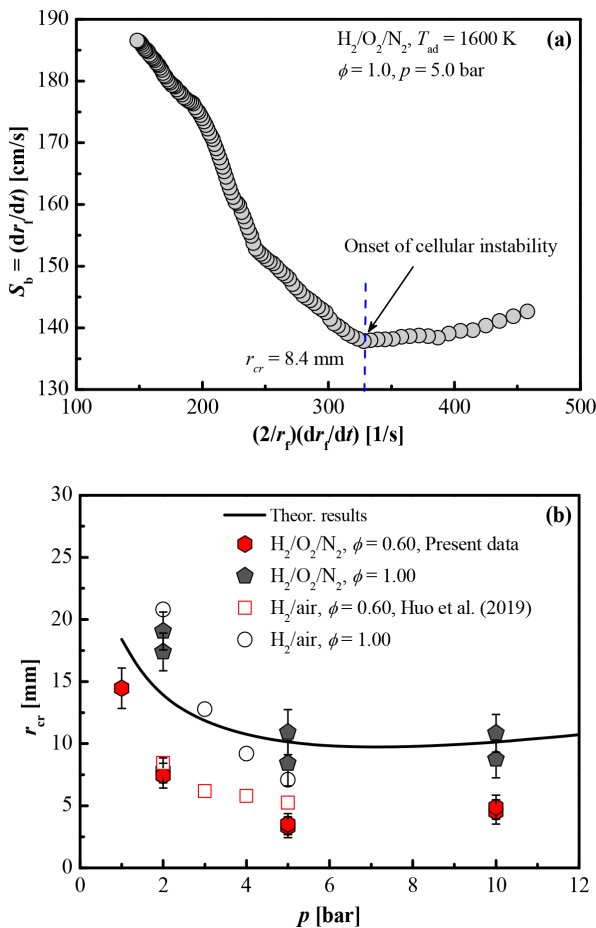


FIG. 10. Measurements of critical radius for the onset of flame cellular instability: (a) determination of critical radius for flame acceleration and (b) critical radius from the experiment and the theory for hydrogen flames at different equivalences ratios and initial pressures. The additional data in (b) are taken from Huo *et al.*⁶⁴

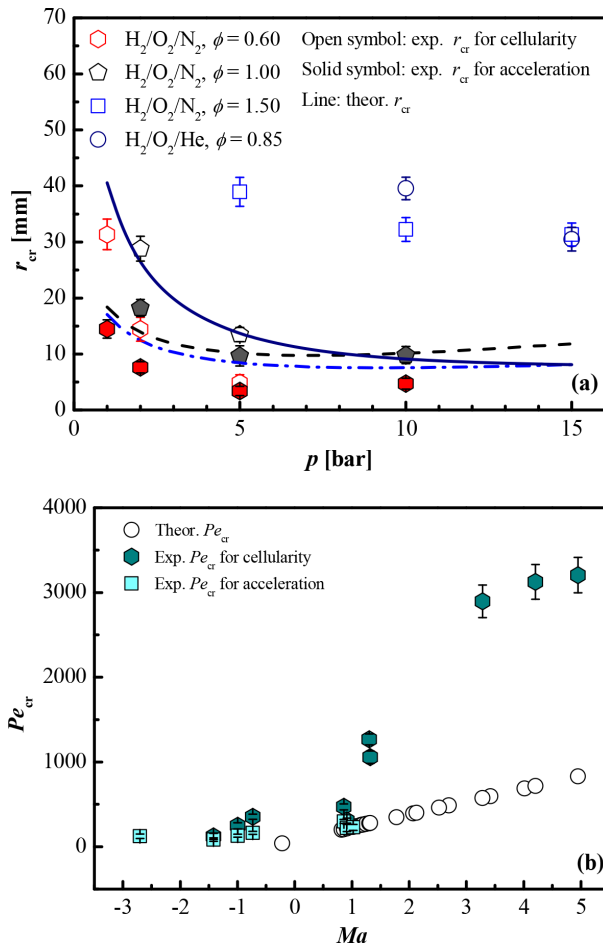


FIG. 11. Comparison of experimental and theoretical critical radii (a) and critical Peclet numbers (b) for the onset of flame cellular instability. The mean experimental values are plotted in the figures for clarity.

for fuel-rich ($\phi = 1.8$) H_2 /air flame at different initial pressures (5–15 bar), which is consistent with the findings in the present work. The theoretical results are 4–5 times smaller than the experimental measurements in both present and previous works for hydrogen flames with $Le_{eff} > 1$. It should be noted that varying definition of flame thickness would decrease the experimental Pe_{cr} . However, it would be not accurate to arbitrary change these parameters for the stability analysis.⁴⁴ The results reveal that linear stability theory can well predict the DL instability but cannot quantitatively predict the DT effects on the developments of cellular structures. Then, the theory under-predicts the Pe_{cr} for the onset of cellular instability for off-unity Le_{eff} flames.

D. Self-similar propagation and acceleration exponent

The cells on the flame-front grow quickly and split into multiple new cells as the cellular unstable flame propagates outwardly. The new cells grow as the splitting process finishes as the flame expands. The total flame surface area and the propagation speed increase continuously as the cascading process occurs. Therefore, the self-acceleration

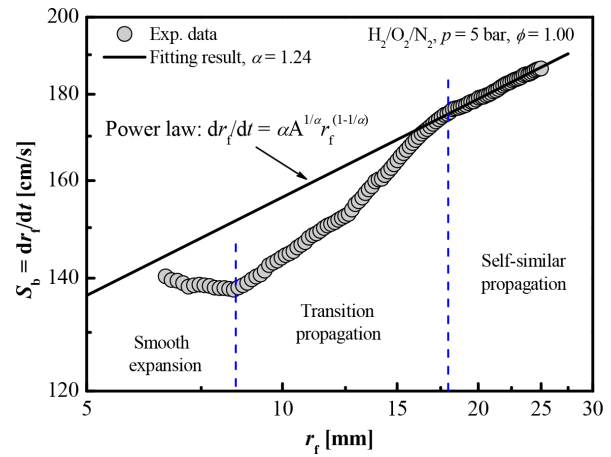


FIG. 12. Three distinct propagation stages of $H_2/O_2/N_2$ flame with cellular instability at $p = 5$ bar and $\phi = 1.00$.

of the cellular unstable flame is achieved. The self-acceleration can be described by the power-law relation, $r_f = r_0 + t^\alpha$, which can be further arranged as $dr_f/dt = \alpha A^{1/\alpha} r_f^{(1-1/\alpha)}$. The fractal excess, $d = 1 - 1/\alpha$, would be used to assess if self-turbulization of the flames is achieved. A fully developed Kolmogorov turbulence has the fractal dimension, D of $7/3$, where the $D = 2 + d$. Analogous to the turbulence, the flame is expected to be self-turbulization if the $d = 0.33$ and $\alpha = 1.5$.

Figure 12 shows the flame propagation speed with the flame radius for stoichiometric $H_2/O_2/N_2$ flame at 5 bar. Three distinct propagation stages are observed, namely, smooth expansion, transition propagation, and self-similar propagation. The slope in the transition propagation stage is higher than that in the self-similar propagation stage, which agrees with the previous experimental observations.^{35,36} The acceleration exponent, α , can be extracted based on the power-law of $dr_f/dt = \alpha A^{1/\alpha} r_f^{(1-1/\alpha)}$ in the self-similar propagation stage. This method was recommended by Wu *et al.*³⁴ to eliminate the ignition effects on fitting the $r_f = r_0 + t^\alpha$. The measured acceleration exponent and fractal excess for cellular unstable hydrogen flames are plotted in Fig. 13. It is seen that both α and d are insensitive to the initial pressure and equivalence ratio. It suggests that the α and d in the self-similar propagation stage are independent of the initial pressure and Lewis number, at least for present experiments. This phenomenon was also observed by Yang *et al.*³⁵ and Huo *et al.*³⁶ using the same extraction method. In our recent work,⁴³ the local α is demonstrated to increase gradually with the r_f or Pe , and the α at $Pe = e^2 Pe_{cr}$ in the self-similar propagation stage is almost a constant value under different Le_{eff} , δ_F , and σ . In addition, the experimental measured α and d from Huo *et al.*³⁶ are consistent with the present results, as shown in Fig. 13. The values of the α are located between 1.22 and 1.40 and the corresponding d within 0.18 and 0.29, which are slightly smaller than 1.5 and 0.33, respectively. Therefore, the self-turbulization is not reached in present experiments.

IV. CONCLUSIONS

In this study, the onset of cellular instability and self-similarity of hydrogen expanding spherical flames have been investigated from the results of well-controlled experiments at high pressures. The onset and

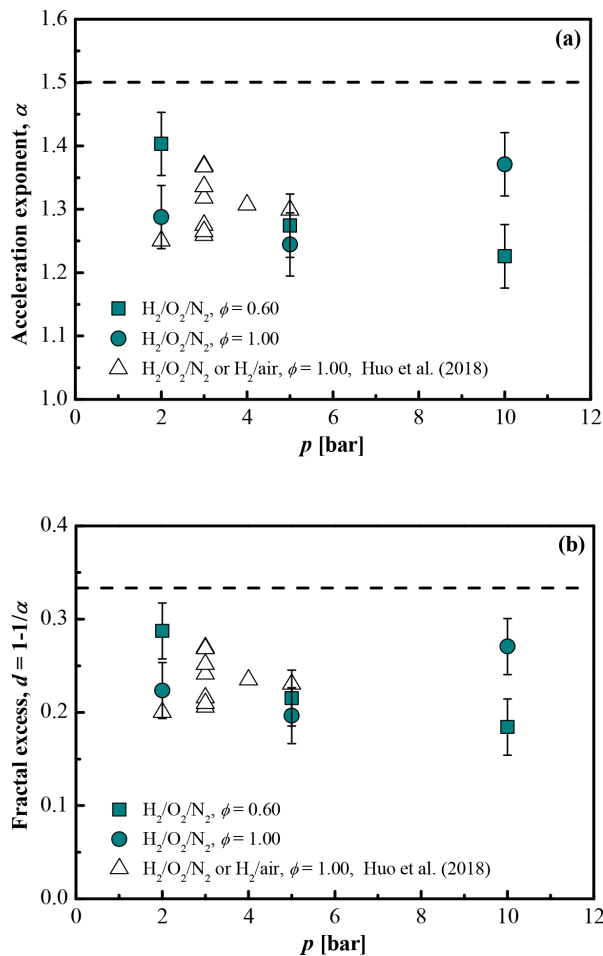


FIG. 13. Experimental acceleration exponent (a) and fractal excess and (b) for hydrogen flames at different initial pressures and equivalence ratios.

growth rate of cellular structures were theoretically analyzed using linear stability theory and compared with the experimental results. In addition, the acceleration exponents of fully developed cellular flames were determined. The key findings are summarized as follows:

- (1) The experimental critical radius, r_{cr} , for flame acceleration varies non-monotonously with the initial pressure for fuel-lean and stoichiometric $H_2/O_2/N_2$ flames. This non-monotonous pressure dependence of the r_{cr} is well captured by linear stability theory, and it is mainly attributed to the thickened flame thickness caused by three-body reaction at very high pressure.
- (2) A quantitative agreement between experimental critical Peclet number, Pe_{cr} , and theoretical predictions is obtained for mixtures with near-unity Lewis number, based on the instant of flame acceleration in experimental measurements and the flame properties following their original definitions in theoretical calculations. However, the linear theory under-predicts the experimental Pe_{cr} for mixtures with off-unity Le_{eff} . The theoretical values are 4 to 5 times smaller than the experimental Pe_{cr} for flame cellularity for hydrogen flames with $Le_{eff} > 1$.

- (3) Three distinct propagation stages are observed for unstable flames, namely, smooth expansion, transition propagation, and self-similar propagation. The acceleration exponent, α , and the corresponding fractal excess, $d = 1 - 1/\alpha$, in the self-similar propagation stage are measured to be within 1.22–1.40 and 0.18–0.29, respectively, which are slightly smaller than the values ($\alpha = 1.5$, $d = 0.33$) associated with flame self-turbulization.

ACKNOWLEDGMENTS

This work is financially supported by the National Natural Science Foundation of China (Nos. 52106183 and 52076171), the China Postdoctoral Science Foundation (No. 2021M692536), and the Fundamental Research Funds for the Central Universities for Xi'an Jiaotong University (No. xzy012022069). The design of the present constant-pressure, dual-chamber vessel is supported by Professor Chung K. Law at Princeton University.

AUTHOR DECLARATIONS

Conflict of Interest

The authors have no conflicts to disclose.

Author Contributions

Xiao Cai: Conceptualization (lead); Data curation (equal); Funding acquisition (equal); Investigation (lead); Methodology (equal); Validation (equal); Writing – original draft (lead); Writing – review & editing (equal). **Limin Su:** Data curation (equal); Investigation (equal). **Jinhua Wang:** Conceptualization (equal); Funding acquisition (equal); Supervision (equal); Writing – review & editing (equal). **Erjiang Hu:** Formal analysis (equal); Methodology (equal). **Zuohua Huang:** Conceptualization (equal); Methodology (equal); Project administration (equal); Supervision (equal).

DATA AVAILABILITY

The data that support the findings of this study are available from the corresponding author upon reasonable request.

REFERENCES

- ¹V. V. Bychkov and M. A. Liberman, “Stability of a flame in a closed chamber,” *Phys. Rev. Lett.* **78**, 1371 (1997).
- ²L. Kagan and G. Sivashinsky, “Transition to detonation of an expanding spherical flame,” *Combust. Flame* **175**, 307 (2017).
- ³Z. Liu, V. R. Unni, S. Chaudhuri, R. Sui, C. K. Law, and A. Saha, “Self-turbulization in cellularly unstable laminar flames,” *J. Fluid Mech.* **917**, A53 (2021).
- ⁴W. Han, C. Wang, and C. K. Law, “Role of transversal concentration gradient in detonation propagation,” *J. Fluid Mech.* **865**, 602 (2019).
- ⁵Z. Huang and H. Zhang, “Ignition and deflagration-to-detonation transition modes in ethylene/air mixtures behind a reflected shock,” *Phys. Fluids* **34**, 086105 (2022).
- ⁶H. Zheng, W. Zhu, X. Jia, and N. Zhao, “Eulerian–Lagrangian modeling of deflagration to detonation transition in n-decane/oxygen/nitrogen mixtures,” *Phys. Fluids* **34**, 126110 (2022).
- ⁷J. Chambers, H. M. Chin, A. Y. Poludnenko, V. N. Gamezo, and K. A. Ahmed, “Spontaneous runaway of fast turbulent flames for turbulence-induced deflagration-to-detonation transition,” *Phys. Fluids* **34**, 015114 (2022).
- ⁸X. Zhao, J. Wang, L. Gao, J. Pan, and Y. Zhu, “Effect of hydrogen concentration distribution on flame acceleration and deflagration-to-detonation transition in staggered obstacle-laden channel,” *Phys. Fluids* **35**, 016124 (2023).

- ⁹V. V. Bychkov and M. A. Liberman, "Dynamics and stability of premixed flames," *Phys. Rep.* **325**, 115 (2000).
- ¹⁰F. Oppong, Z. Luo, X. Li, Y. Song, and C. Xu, "Intrinsic instability of different fuels spherically expanding flames: A review," *Fuel Process. Technol.* **234**, 107325 (2022).
- ¹¹J. K. Bechtold and M. Matalon, "Hydrodynamic and diffusion effects on the stability of spherically expanding flames," *Combust. Flame* **67**, 77 (1987).
- ¹²R. Addabbo, J. K. Bechtold, and M. Matalon, "Wrinkling of spherically expanding flames," *Proc. Combust. Inst.* **29**, 1527 (2002).
- ¹³M. Matalon, "Intrinsic flame instabilities in premixed and nonpremixed combustion," *Annu. Rev. Fluid Mech.* **39**, 163 (2007).
- ¹⁴G. I. Siv Ashinsky, *Nonlinear Analysis of Hydrodynamic Instability in Laminar Flames—I. Derivation of Basic Equations* (Academic Press, San Diego, 1988).
- ¹⁵G. I. Sivashinsky, "Instabilities, pattern formation, and turbulence in flames," *Annu. Rev. Fluid Mech.* **15**, 179 (1983).
- ¹⁶L. Filyand, G. I. Sivashinsky, and M. L. Frankel, "On self-acceleration of outward propagating wrinkled flames," *Physica D* **72**, 110 (1994).
- ¹⁷S. I. Blinnikov and P. V. Sasorov, "Landau-Darrieus instability and the fractal dimension of flame fronts," *Phys. Rev. E* **53**(5), 4827 (1996).
- ¹⁸B. Galanti, O. Kupervasser, Z. Olami, and I. Procaccia, "Dynamics and wrinkling of radially propagating fronts inferred from scaling laws in channel geometries," *Phys. Rev. Lett.* **80**, 2477 (1998).
- ¹⁹K.-L. Pan and R. Fursenko, "Characteristics of cylindrical flame acceleration in outward expansion," *Phys. Fluids* **20**, 094107 (2008).
- ²⁰K. Mukaiyama, S. Shibayama, and K. Kuwana, "Fractal structures of hydrodynamically unstable and diffusive-thermally unstable flames," *Combust. Flame* **160**, 2471 (2013).
- ²¹M. A. Liberman, M. F. Ivanov, O. E. Peil, D. M. Valiev, and L.-E. Eriksson, "Self-acceleration and fractal structure of outward freely propagating flames," *Phys. Fluids* **16**, 2476 (2004).
- ²²J. Yuan, Y. Ju, and C. K. Law, "Coupled hydrodynamic and diffusional-thermal instabilities in flame propagation at subunity Lewis numbers," *Phys. Fluids* **17**, 074106 (2005).
- ²³Y. X. Xin, C. S. Yoo, J. H. Chen, and C. K. Law, "A DNS study of self-accelerating cylindrical hydrogen-air flames with detailed chemistry," *Proc. Combust. Inst.* **35**, 753 (2015).
- ²⁴R. Yu, X.-S. Bai, and V. Bychkov, "Fractal flame structure due to the hydrodynamic Darrieus-Landau instability," *Phys. Rev. E* **92**, 063028 (2015).
- ²⁵L. Berger, K. Kleinheinz, A. Attili, and H. Pitsch, "Characteristic patterns of thermodynamically unstable premixed lean hydrogen flames," *Proc. Combust. Inst.* **37**, 1879 (2019).
- ²⁶D. Bradley and C. M. Harper, "The development of instabilities in laminar explosion flames," *Combust. Flame* **99**, 562 (1994).
- ²⁷D. Bradley, C. G. W. Sheppard, R. Woolley, D. A. Greenhalgh, and R. D. Lockett, "The development and structure of flame instabilities and cellularity at low Markstein numbers in explosions," *Combust. Flame* **122**, 195 (2000).
- ²⁸D. Bradley, T. M. Cresswell, and J. S. Puttock, "Flame acceleration due to flame-induced instabilities in large-scale explosions," *Combust. Flame* **124**, 551 (2001).
- ²⁹D. Bradley, M. Lawes, K. Liu, S. Verhelst, and R. Woolley, "Laminar burning velocities of lean hydrogen-air mixtures at pressures up to 1.0 MPa," *Combust. Flame* **149**, 162 (2007).
- ³⁰D. Bradley, M. Lawes, R. Mumby, and P. Ahmed, "The stability of laminar explosion flames," *Proc. Combust. Inst.* **37**, 1807 (2019).
- ³¹O. C. Kwon, G. Rozenchan, and C. K. Law, "Cellular instabilities and self-acceleration of outwardly propagating spherical flames," *Proc. Combust. Inst.* **29**, 1775 (2002).
- ³²C. K. Law, G. Jomaas, and J. K. Bechtold, "Cellular instabilities of expanding hydrogen/propane spherical flames at elevated pressures: Theory and experiment," *Proc. Combust. Inst.* **30**, 159 (2005).
- ³³G. Jomaas, C. K. Law, and J. K. Bechtold, "On transition to cellularity in expanding spherical flames," *J. Fluid Mech.* **583**, 1–26 (2007).
- ³⁴F. Wu, G. Jomaas, and C. K. Law, "An experimental investigation on self-acceleration of cellular spherical flames," *Proc. Combust. Inst.* **34**, 937 (2013).
- ³⁵S. Yang, A. Saha, F. Wu, and C. K. Law, "Morphology and self-acceleration of expanding laminar flames with flame-front cellular instabilities," *Combust. Flame* **171**, 112 (2016).
- ³⁶J. Huo, A. Saha, Z. Ren, and C. K. Law, "Self-acceleration and global pulsation in hydrodynamically unstable expanding laminar flames," *Combust. Flame* **194**, 419 (2018).
- ³⁷Z. Liu, V. R. Unni, S. Chaudhuri, C. K. Law, and A. Saha, "Local statistics of laminar expanding flames subjected to Darrieus-Landau instability," *Proc. Combust. Inst.* **38**, 1993 (2021).
- ³⁸S. Yang, A. Saha, Z. Liu, and C. K. Law, "Role of Darrieus-Landau instability in propagation of expanding turbulent flames," *J. Fluid Mech.* **850**, 784 (2018).
- ³⁹J. Wang, Y. Xie, X. Cai, Y. Nie, C. Peng, and Z. Huang, "Effect of H₂O addition on the flame front evolution of syngas spherical propagation flames," *Combust. Sci. Technol.* **188**, 1054 (2016).
- ⁴⁰Y. Xie, J. Wang, X. Cai, and Z.-H. Huang, "Self-acceleration of cellular flames and laminar flame speed of syngas/air mixtures at elevated pressures," *Int. J. Hydrogen Energy* **41**, 18250 (2016).
- ⁴¹X. Cai, J. Wang, H. Zhao, M. Zhang, and Z.-H. Huang, "Flame morphology and self-acceleration of syngas spherically expanding flames," *Int. J. Hydrogen Energy* **43**, 17531 (2018).
- ⁴²H. Zhao, J. Wang, Z. Bian, X. Cai, X. Li, and Z. Huang, "Onset of cellular instability and self-acceleration propagation of syngas spherically expanding flames at elevated pressures," *Int. J. Hydrogen Energy* **44**, 27995 (2019).
- ⁴³X. Cai, J. Wang, Z. Bian, H. Zhao, H. Dai, and Z. Huang, "On transition to self-similar acceleration of spherically expanding flames with cellular instabilities," *Combust. Flame* **215**, 364 (2020).
- ⁴⁴J. Beckmann, R. Hesse, S. Kruse, A. Berens, N. Peters, H. Pitsch, and M. Matalon, "Propagation speed and stability of spherically expanding hydrogen/air flames: Experimental study and asymptotics," *Proc. Combust. Inst.* **36**, 1531 (2017).
- ⁴⁵Y. A. Gostintsev, A. G. Istratov, and Y. V. Shulenin, "Self-similar propagation of a free turbulent flame in mixed gas mixtures," *Combust., Explos. Shock Waves* **24**, 563 (1989).
- ⁴⁶Y. A. Gostintsev, V. E. Fortov, and Y. V. Shatskikh, "Self-similar propagation law and fractal structure of the surface of a free expanding turbulent spherical flame," *Dokl. Phys. Chem.* **397**, 141 (2004).
- ⁴⁷M. Z. Haq, "Correlations for the onset of instabilities of spherical laminar premixed flames," *J. Heat Transfer* **127**, 1410 (2005).
- ⁴⁸C. R. Bauwens, J. M. Berghorson, and S. B. Dorofeev, "Experimental study of spherical-flame acceleration mechanisms in large-scale propane-air flames," *Proc. Combust. Inst.* **35**, 2059 (2015).
- ⁴⁹W. K. Kim, T. Mogi, K. Kuwana, and R. Dobashi, "Self-similar propagation of expanding spherical flames in large scale gas explosions," *Proc. Combust. Inst.* **35**, 2051 (2015).
- ⁵⁰X. Lu, E. Hu, Z. Xu, R. Ge, Z. Huang, and K. Zeng, "Non-monotonic behavior of flame instability of 1,3-butadiene/O₂/He mixture up to 1.5 MPa," *Fuel* **255**, 115749 (2019).
- ⁵¹X. Lu, E. Hu, S. Huang, Z. Xu, X. Li, and Z. Huang, "Experimental and kinetic study on laminar burning velocities of 1,3-butadiene at pressures up to 1.5 MPa," *Fuel* **246**, 222 (2019).
- ⁵²M. P. Burke, Z. Chen, Y. Ju, and F. L. Dryer, "Effect of cylindrical confinement on the determination of laminar flame speeds using outwardly propagating flames," *Combust. Flame* **156**, 771 (2009).
- ⁵³Z. Chen, "On the extraction of laminar flame speed and Markstein length from outwardly propagating spherical flames," *Combust. Flame* **158**, 291 (2011).
- ⁵⁴X. Cai, J. Wang, H. Zhao, Y. Xie, and Z. Huang, "Effects of initiation radius selection and Lewis number on extraction of laminar burning velocities from spherically expanding flames," *Combust. Sci. Technol.* **190**, 286 (2017).
- ⁵⁵M. P. Burke, M. Chaos, F. L. Dryer, and Y. Ju, "Negative pressure dependence of mass burning rates of H₂/CO/O₂/diluent flames at low flame temperatures," *Combust. Flame* **157**, 618 (2010).
- ⁵⁶J. K. Bechtold and M. Matalon, "The dependence of the Markstein length on stoichiometry," *Combust. Flame* **127**, 1906 (2001).
- ⁵⁷C. K. Law and C. J. Sung, "Structure, aerodynamics, and geometry of premixed flamelets," *Prog. Energy Combust. Sci.* **26**, 459 (2000).
- ⁵⁸A. G. Istratov and V. B. Librovich, "On the stability of gasdynamic discontinuities associated with chemical reactions. The case of a spherical flame," *Astronaut. Acta* **14**, 453 (1969).
- ⁵⁹A. G. Class, B. J. Matkowsky, and A. Y. Klimenko, "A unified model of flames as gasdynamic discontinuities," *J. Fluid Mech.* **491**, 11 (2003).

- ⁶⁰G. K. Giannakopoulos, A. Gatzoulis, C. E. Frouzakis, M. Matalon, and A. G. Tomboulides, "Consistent definitions of 'flame displacement speed' and 'Markstein length' for premixed flame propagation," *Combust. Flame* **162**, 1249 (2015).
- ⁶¹S. Kwon, L. K. Tseng, and G. M. Faeth, "Laminar burning velocities and transition to unstable flames in $H_2/O_2/N_2$ and $C_3H_8/O_2/N_2$ mixtures," *Combust. Flame* **90**, 230 (1992).
- ⁶²P. Clavin and G. Joulin, *Flamelet Library for Turbulent Wrinkled Flames* (Springer US, New York, NY, 1989).
- ⁶³F. Oppong, C. Xu, L. Zhongyang, X. Li, W. Zhou, and C. Wang, "Cellularization of 2-methylfuran expanding spherical flame," *Combust. Flame* **206**, 379 (2019).
- ⁶⁴J. Huo, A. Saha, T. Shu, Z. Ren, and C. K. Law, "Self-acceleration and global pulsation in expanding laminar $H_2-O_2-N_2$ flames," *Phys. Rev. Fluids* **4**, 043201 (2019).